INTERNATIONAL JOURNAL FOR NUMERICAL METHODS IN FLUIDS, VOL. 4, 207–229 (1984)

COATING FLOW THEORY BY FINITE ELEMENT AND ASYMPTOTIC ANALYSIS OF THE NAVIER–STOKES SYSTEM*

S. F. KISTLER AND L. E. SCRIVEN

Department of Chemical Engineering & Materials Science, University of Minnesota, Minneapolis, MN 55455 U.S.A.

SUMMARY

Coating flows are laminar free surface flows, preferably steady and two-dimensional, by which a liquid film is deposited on a substrate. Their theory rests on mass and momentum accounting for which Galerkin's weighted residual method, finite element basis functions, isoparametric mappings, and a new free surface parametrization prove particularly well-suited, especially in coping with the highly deformed free boundaries, irregular flow domains, and the singular nature of static and dynamic contact lines where fluid interfaces intersect solid surfaces. Typically, short forming zones of rapidly rearranging two-dimensional flow merge with simpler asymptotic regimes of developing or developed flow upstream and downstream. The two-dimensional computational domain can be shrunk in size by imposing boundary conditions from asymptotic analysis of those regimes or by matching to one-dimensional finite element solutions of asymptotic equations.

The theory is laid out with special attention to conditions at free surfaces, contact lines, and open inflow and outflow boundaries. Efficient computation of predictions is described with emphasis on a grand Newton iteration that converges rapidly and brings other benefits. Sample results for curtain coating and roll coating flows of Newtonian liquids illustrate the power and effectiveness of the theory.

KEY WORDS Coating Flows Viscous Flows Free Surfaces Free Boundaries Boundary Parameterization Moving Spine Method

INTRODUCTION

The purpose of a coating flow is to deposit a thin and uniform liquid film—in some cases a film stratified in composition—on a flexible sheet or solid substrate. Therefore, a coating flow is a laminar free surface flow. A successful coating flow is steady and it is two-dimensional, except for narrow edge regions.

Examples of coating flows diagrammed in Figure 1 range from rimming flow, with which our coating flow theory began,[1,2] to reverse roll coating and curtain coating, which are featured below. In rimming flow, a limited amount of liquid is put inside the tube or cylinder to be coated, which is oriented horizontally and spun about its axis so that the liquid forms a continuous film. There is neither inflow nor outflow, but closed flow. Nor are there contact lines where the liquid/gas interface intersects the solid surface. Because it requires neither upstream nor downstream boundary conditions nor knowledge of the physics of static and dynamic contact lines, and because it has limiting regimes that can be analysed by conventional perturbation methods, rimming flow proved an apt starting point. In much-studied

* This invited paper is an extended and refereed version of one presented at the Fourth International Symposium on Finite Elements in Flow Problems held in Tokyo, Japan, 26–29 July 1982.

0271–2091/84/030207–23$02.30 *Received 18 January 1983*

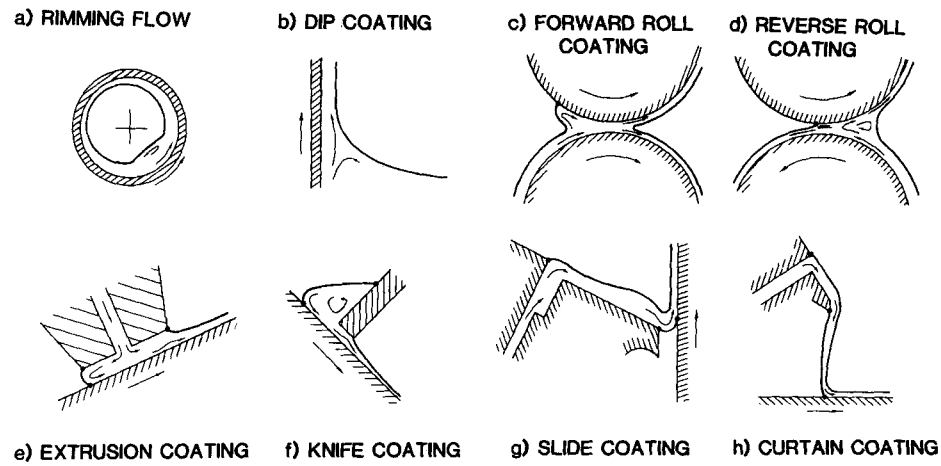

Figure 1. Schematic of selected coating operations

dip-coating there is the complication of upstream inflow and downstream outflow, but still no contact lines in the film-forming zones. In other coating flows the contact lines are present, as indicated in Figure 1. The physics of flow at and near static contact lines, or separation lines, and dynamic contact lines, or wetting lines, was not known at the outset and, because it is still not fully elucidated, remains one of the active areas of scientific research about coating flows.

The hallmarks of coating flows are the irregular flow domains and deformed free boundaries that rarely conform to the co-ordinate surfaces of any convenient co-ordinate system. These are prominent in the forming zones, which are the comparatively short regions of rapidly rearranging shear and extensional flow. Standard fluid mechanical approximations rarely apply, because viscous, pressure and capillary forces together often with inertial and gravity forces all contend with one another in two-dimensional flow. Typically the forming zones merge with simpler regimes of developing flow and, far upstream and far downstream, regions of fully developed flow. To create a theory from which accurate predictions of such complex flows can be calculated, first of all when the liquid is Newtonian, was the challenge.

The challenge has been met by a strategy of dividing a coating flow into zones, and describing each as economically as consistent accuracy allows: efficient free-surface parametrization and two-dimensional Navier–Stokes equations together with isoparametrically mapped finite element basis functions in the forming zones; one-dimensional asymptotic approximations to the Navier–Stokes system together with finite element basis functions in the developing flow zones; and closed-form solutions in the zones of fully developed flow. Successive zones are of course coupled to their neighbours upstream and downstream, and where the coupling is appreciable the zones must be treated all together in order to arrive at an efficient algorithm for computing predictions. The tactics can be used in other sorts of problems with distinctive zones, free boundaries, or open flow boundaries.

In this paper we illustrate the theory by its application to curtain coating, a coating operation which epitomizes irregular flow domains and deformed free boundaries. At the end we also show some theoretical predictions of roll coating from recent work of Coyle *et al.*[3,4] Additional predictions appear in the extended abstract of the present paper.[5]

ZONES IN COATING FLOWS

Curtain coating, which is archetypal, is usefully divided into the seven zones shown in Figure 2:

1. Feed zone—upstream in the feed slot, where liquid supplied by a manifold in the coating die arrives in plane Poiseuille flow, a fully developed, rectilinear flow in which no influence is transmitted further upstream (except in virtue of the uniform pressure gradient).
2. Film-forming zone—at the slot exit, where liquid turns direction, acquires a free surface which separates from the die at a static contact line, and under gravity begins to flow down the slide face of the die.
3. Film-flow zone—on the slide face, where the liquid film approaches and perhaps attains the fully developed Nusselt flow (semiparabolic velocity distribution), which is devoid of upstream influence.
4. Sheet-forming zone—around the die lip, where the liquid film changes direction and falls off the die, acquiring a second free surface which also separates at a static contact line.
5. Curtain-flow zone—beyond, where the falling liquid sheet approaches and perhaps attains a virtually pure extensional flow regime (irrotational) in which acceleration by gravity contends with upstream influence through normal viscous stress that diminishes downstream.
6. Coated-film-forming zone, or impinging zone—where the falling liquid sheet, or curtain, meets the moving substrate being coated, and displaces the gas previously in contact as it changes direction abruptly, one of the free surfaces appearing to terminate in a dynamic contact line.
7. Take-away zone—downstream, where the coated liquid film approaches and ultimately attains the fully developed plug flow of solid-body translation at the substrate speed, and there is again no upstream influence.

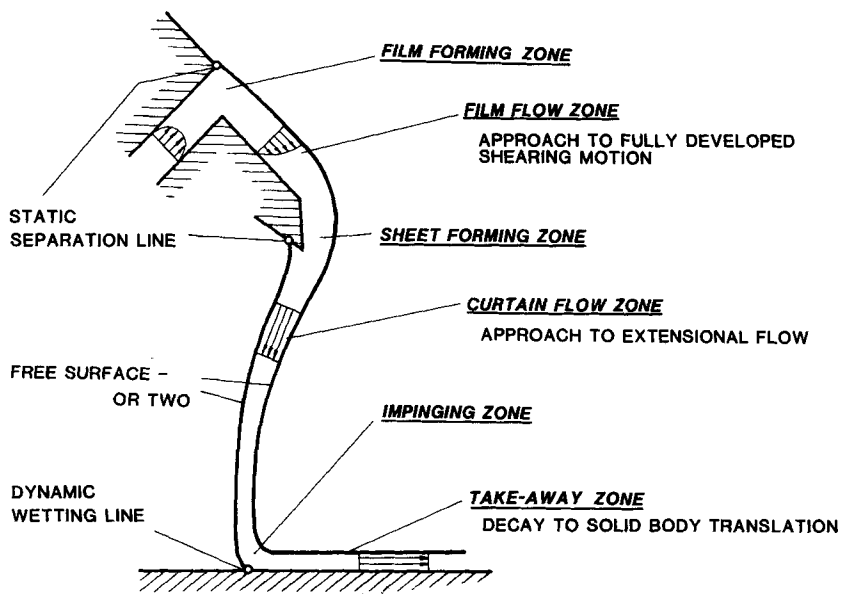

Figure 2. Flow zones in coating: example of curtain coating

The crucial zones are those of fully two-dimensional flow rearrangement and abundant upstream influence: here the film-forming zone, the sheet-forming zone and the impinging zone.

How many of these zones to consider at once is a matter of the strength of upstream influence, i.e. normal viscous stress and varying pressure gradient—especially any gradient of capillary pressure, the resultant of surface tension acting in a curved free surface. Here these effects are weak in the film-flow zone and the curtain-flow zone, and hence the theory can be divided there (the treatment of the film-forming zone is not taken up below, but see References 6 and 7).

GOVERNING EQUATIONS

As an illustrative case the steady, incompressible, isothermal flow of liquid in the forming zone of the coated liquid film is considered: see Figure 3. The governing equations are made non-linear by the convective term when the Reynolds number is not vanishingly small, and always by an unknown free surface. The formulation of the problem in the sheet-forming zone is similar, except that there is a static contact line and no dynamic one.

In analysing the impinging zone the velocity of the inflowing curtain can be taken as known, and so can its position relative to the coating die. The flow is of course governed by the momentum and continuity principles, shown in Figure 3 in the dimensionless form of their pointwise versions. Length is measured in units of the ultimate thickness of the coated film, h_∞. $\mathbf{v}$ is velocity measured in units of substrate speed U. $\mathbf{T}$ is the stress tensor, here taken to be that of Newtonian liquid ($\mathbf{T}=-\mathbf{I}p+[\nabla\boldsymbol{v}+(\nabla\boldsymbol{v})^T]$), and is measured in units of $\mu U/h_\infty$, where μ is viscosity. $Re\equiv\rho Uh_\infty/\mu$ is the Reynolds number and $St\equiv\mu U/\rho gh_\infty^2$ is the Stokes number. $\mathbf{f}$ is a unit vector in the direction of the force of gravity.

At internal interfaces between stratified layers of different viscosity in multilayer coating (touched on below) the momentum principle requires continuous traction, i.e. $\mathbf{n}\cdot\mathbf{T}_A = m\mathbf{n}\cdot\mathbf{T}_B$ when, as is usual, the layers are miscible; $m\equiv\mu_B/\mu_A$ is the ratio of viscosities of layer B and layer A (a similar condition can be used to account for air drag). The continuity and no-slip conditions of course require $\mathbf{v}_A=\mathbf{v}_B$.

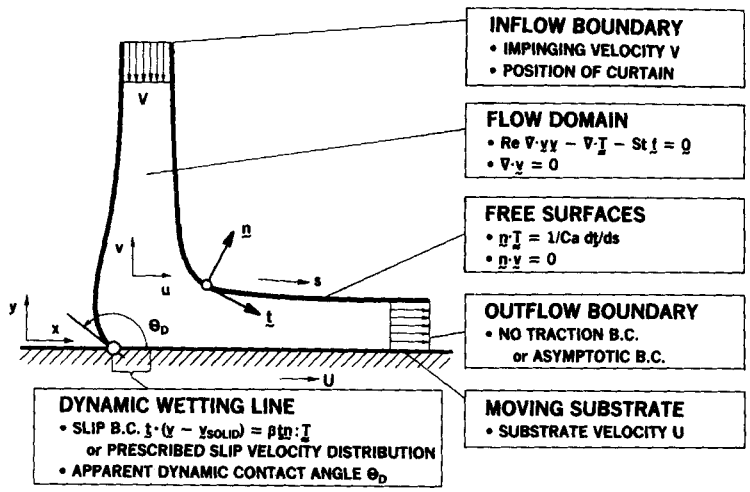

Figure 3. Impinging zone in curtain coating, with governing equations and boundary conditions

At free surfaces the momentum principle requires that normal stress in the liquid (relative to pressure in the gas, which is here taken as inviscid and inertia-free) balance any capillary pressure, as seen in Figure 3. Capillary pressure requires a curved free surface and hence a unit tangent $\mathbf{t}$ that varies with distance s along the surface. The magnitude of the ratio of the contending stresses is measured by the capillary number, $Ca \equiv \mu U/\sigma$, where σ denotes surface tension.

At free surfaces the continuity principle requires that there be no flow across the surface, which is the familiar kinematic boundary condition $\mathbf{n} \cdot \mathbf{v} = 0$, $\mathbf{n}$ being the unit normal.

At some chosen outflow 'boundary' far enough downstream on the moving substrate the flow is fully developed translation and so the mass and momentum fluxes are known there. Or else at an outflow 'boundary' chosen closer the further relaxation of the developing flow into such a state can be described by a boundary condition of the third kind, which is derived from asymptotic analysis of the relaxation process.[8,9]

At the surface of a solid or flexible substrate there is neither slip nor penetration, and so the liquid velocity is that of the substrate. The neighbourhood of the dynamic contact line, or wetting line, is an exception. There the momentum principle requires some slip if the situation is idealized as steady, two-dimensional, complete displacement of the air originally in contact with the substrate.[10–12] Otherwise a non-integrable stress singularity arises in the abrupt change in boundary conditions at the putative line.[13] The slip can be described by Navier's old boundary condition with slip coefficient β ($1/\beta$ is the transfer coefficient for tangential momentum), which is a boundary condition of the third kind, or by prescribing an equivalent distribution of slip velocity in a condition of the first kind.[13–15] There is a length parameter, $\beta\mu$ in the first case, that measures the extent of substrate surface where slip is significant.

At the wetting line the momentum principle also requires specifying the fluid mechanically apparent dynamic contact angle θ_D, unless the capillary number is high. High capillary number implies that the effect of capillary pressure, and hence of free surface curvature, is restricted to a scale smaller than that on which the wetting line appears to exist. The dynamic contact angle is then a dependent variable. This is so in the sample results below for the impinging zone.

Asymptotic analysis of the stress singularity caused by the no-slip condition at static contact lines, as in the sheet-forming zone, indicates that the singularity is integrable, i.e. the total force exerted by the liquid on the solid remains bounded, and so there is no need to admit slip.[16,15] If a static contact line does not remain pinned at a sharp corner or compositional discontinuity but rather is free to migrate, an apparent static contact angle θ_C has to be specified. This angle seems unaffected by changes in the adjacent flow field.[17]

Such problems as posed here have, heretofore, been locked away from solution. There is a set of keys to solving them. The first is finite element basis functions. The second is Galerkin's method of weighted residuals. Another is efficient description, or parametrization, of free boundaries. Another is isoparametric mapping by the finite element basis functions onto a fixed computational domain. The most novel aspect of coating flow theory is the parametrization of free boundaries and the related tessellation of the flow domain into subdomains on which the governing equations are solved by the Galerkin/finite element method.

FREE BOUNDARY PARAMETRIZATION AND DOMAIN TESSELLATION

To calculate a prediction of curtain coating requires iteration to solve the non-linear set of governing equations. Crucial to reliable, efficient readjustment of free boundaries at each

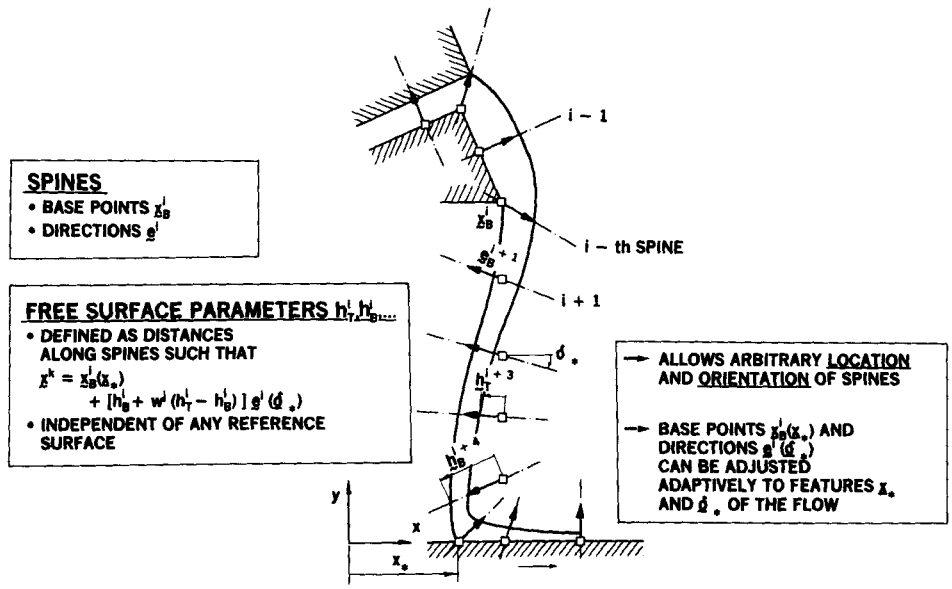

Figure 4. Free boundary parametrization by means of spines

step of the iteration are the flexibility and simplicity of their parametrization and of the associated tessellation of the flow domain into finite elements. Major advances were Ruschak's boundary supports[18] and then the simple idea of spines.[5,19] Spines are conveniently located and oriented lines (or curves), is indicated in Figure 4; each is defined by a base point $\mathbf{x}_B^i$ and a direction $\mathbf{e}^i$. Along a spine the distance from the base point to a free surface or interface, e.g. h_B^i, h_T^i or h_I^i, is the free surface's or interface's local co-ordinate, an unknown to be solved for (along a spine the distance to a rigid wall is the rigid wall's local co-ordinate, which is known). There is no reference surface and the dangers of a reference surface are avoided: spines can be located and oriented to accommodate highly irregular configurations without the free surface representation becoming singular.

The base points and directions can be made to follow adaptively and automatically such features as the location x_* of the dynamic contact line and the inclination δ_* of a zone's inflow or outflow plane (where flux-matching conditions are to be imposed). The set of features $\mathbf{x}_*$ on which base points depend, and the set $\boldsymbol{\delta}_*$ on which orientations depend, become parameters in the base point locations and directions, e.g. $\mathbf{x}_B^i(\mathbf{x}_*)$ and $\mathbf{e}^i(\boldsymbol{\delta}_*)$, and can be taken as unknowns in the iterations and continuations described below if functional requirements are imposed on them.

In conjunction with spine placement the flow domain is tessellated into quadrilateral elements (triangles can be employed as well), as shown in Figure 5. Two opposing sides of each element are defined by spines. The other two sides are made to intersect those spines at fixed relative locations w^j between the boundary surfaces (see also Figure 4); these sides are then interpolated between the spines by isoparametric transformation of a standard quadrilateral, namely a square. Thus many of the elements have two curved sides that reflect free surfaces.

The intersections are the vertex nodes of elements. Other nodes likewise lie on spines at positions given by prescribed proportions w^j of the local thickness of the flow. Thus the

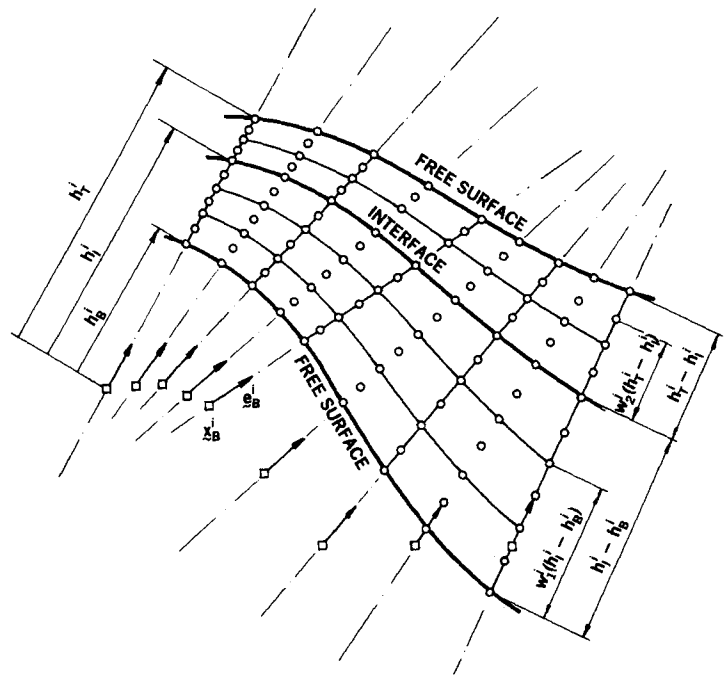

Figure 5. Tessellation of flow domain into finite elements: example of stratified flow with two free surfaces and one interface

location $\mathbf{x}^k(\mathbf{h})$ of node $k(i, j)$ on the ith spine is related to the positions, e.g. h_B^i and h_T^i, of any free surfaces intersected by that spine. The column vector $\mathbf{h}$ denotes the entire set of coefficients and parameters that define free boundary shapes and spine placement, namely $\{\mathbf{h}_B, \mathbf{h}_T, \ldots, \mathbf{x}_*, \boldsymbol{\delta}_*\}$. This scheme is readily extended to accommodate stratified flow, as the example in Figure 5 shows. There the node arrangement is that of the nine-node biquadratic finite element basis functions for velocity and four-node bilinear ones for pressure in a standard 'mixed interpolation' approach[20] that has been used in developing the present theory (three-node linear discontinuous basis functions may be superior for the pressure field[21,22]).

The isoparametric transformations[23,24] of the standard square in the (ξ, η)-plane that produce all of the elements in the flow domain actually define a global map of a complicated curvilinear free surface flow into a rectilinear domain, as shown in Figures 6 and 7, where the parameters (ξ, η) are simple Cartesian co-ordinates. This domain can be called the computational domain. When there is flow splitting, as in roll coating, the computational domain is not a single strip, but has a branched shape corresponding to the way separate families of spines are patched together (Figure 7). In every case the global values of the (ξ, η)-co-ordinates can be suppressed but the adjacency structure of the elements in the physical domain is preserved.

The momentum and continuity equations are in effect solved in the computational domain, the isoparametric mapping onto the physical domain being part of the problem. It is this mapping that locates the free surfaces of the coating flow, in the way described in Figure 6.

The local isoparametric mappings by the biquadratic finite element basis functions make the free surfaces simple one-dimensional quadratic mappings of straight lines, $\eta = \text{constant}$,

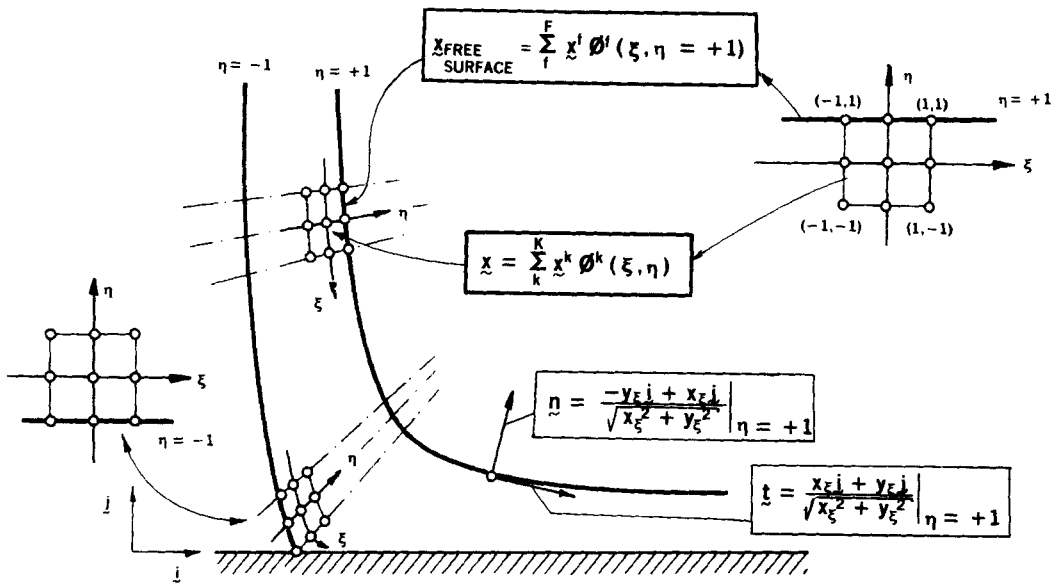

Figure 6. Local map of flow domain and free surfaces by isoparametric mapping

in the computational domain (ξ, η). The result is an expansion of free surface shape in terms of **h**, the set of spine locations and free surface parameters. This is consistent with the expansion of the velocity field and decidely superior to earlier practice (cf. References 15, 25). It is akin to the use of local co-ordinate patches well-known in differential geometry and avoids the need for a reference surface.

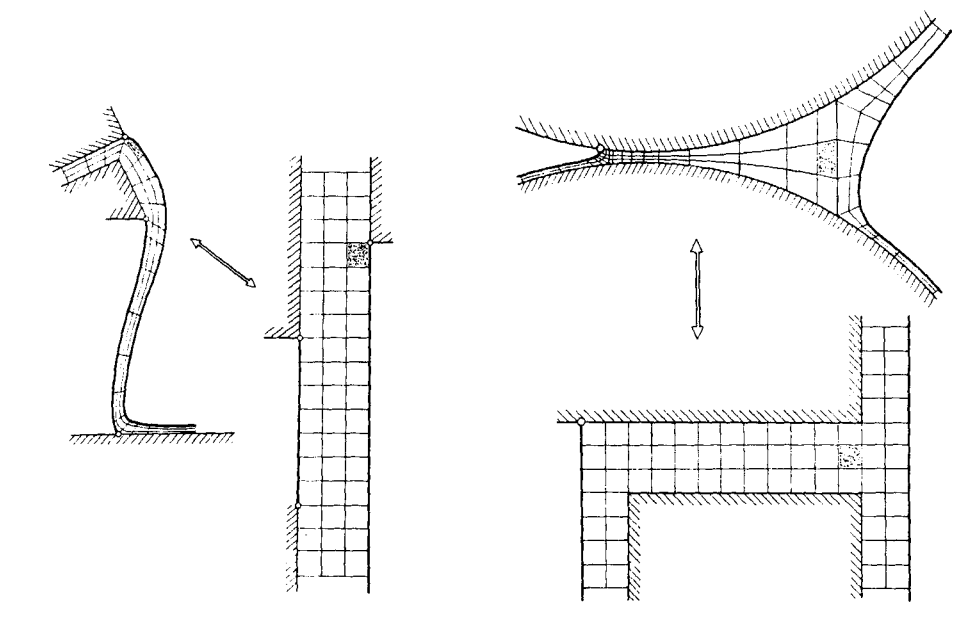

Figure 7. Global map of flow domain and free surfaces by isoparametric mappings

Because the free surfaces are curves of $\eta = +1$ or $\eta = -1$, the formulae for their unit tangent and normal vectors, which are needed for boundary conditions, are simple and computationally convenient. Moreover, evaluated at surface Gauss points (see below) they are consistent with the requirements of conservation of incompressible mass (continuity equation) and impenetrability of the free surface to mass (kinematic boundary condition): cf. Reference 26. These are added benefits from the method of surface parametrization, a key to solving free boundary problems.

GALERKIN WEIGHTED RESIDUAL EQUATIONS

Residuals of the differential equations and boundary conditions that express conservation of mass and momentum are, as usual, made orthogonal to the finite element basis functions used to approximate the pressure and velocity fields and free boundary shapes. The resulting algebraic equations, most of them non-linear, are, of course, the discretized analogue of the original viscous free surface flow problem. Certain aspects warrant mention here; a comprehensive discussion is available elsewhere.[6]

There are advantages in leaving the differential equation of momentum conservation in its natural form, which is in terms of the divergence of the total momentum flux—convective as well as diffusive flux. Then in its weak form, i.e. in the Galerkin weighted momentum residual after the usual invocation of the divergence theorem, the boundary residual can be replaced by the residual of the momentum flux boundary condition. Such residuals are shown in Figure 8 for the free surfaces, for the outflow plane, and for the neighbourhood of the wetting line in the impinging zone, i.e. the slip region. The boundary residual vanishes at the rigid substrate and the inflow plane, where there are essential boundary conditions (it would vanish too on a plane of symmetry, if one were present).

$$\underset{\sim}{R}^k = \int_{\Omega_{DOMAIN}} \{ \nabla \phi^k (-Re\, \underline{v}\underline{v} + \underline{\underline{T}}) - \phi^k St\, \underline{f} \}\, dV - \int_{\partial\Omega_{BOUNDARY}} \phi^k \underline{n} \cdot (-Re\, \underline{v}\underline{v} + \underline{\underline{T}})\, ds = \underline{0}$$

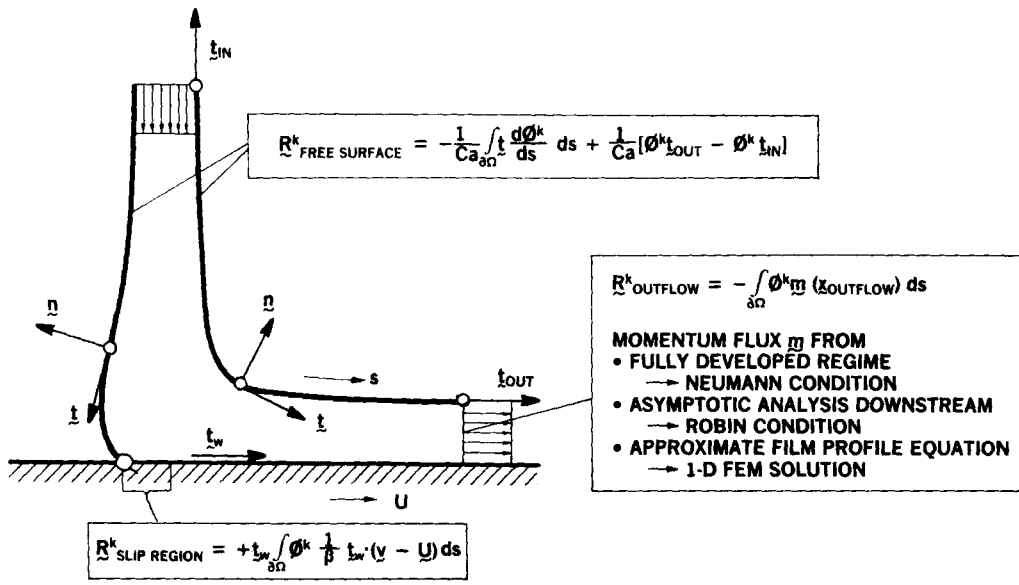

Figure 8. Galerkin weighted momentum residual and boundary contributions

The momentum flux boundary condition at a free surface contains the surface curvature $d\mathbf{t}/ds$, as recorded above. But this curvature can be eliminated in favour of the unit tangent itself, by applying the surface divergence theorem to the residual of the boundary condition, as has been done to arrive at the form in Figure 8. As a consequence, lower-order finite element basis functions, i.e. ones that are piecewise once-differentiable to yield the unit tangent, suffice for the representation of a free surface (the quadratic basis functions actually used are piecewise twice-differentiable). This key tactic is due to Ruschak.[18]

The natural form of the momentum equation also accommodates nicely the slip boundary condition near a wetting line. The size of the slip region and the magnitude of the slip coefficient are empirical inputs and the sensitivity to them of a computed prediction should be evaluated. In the sample results presented below, slip was restricted to the element adjoining the dynamic wetting line and was sufficient that further increase had no appreciable effect outside that element.

The natural form also accommodates the dynamic condition which is demanded by physics at inflow and outflow boundaries: the total momentum flux $\mathbf{m}$ must be continuous. There are three ways of imposing this:

1. If the finite element domain is extended far enough downstream (upstream) to reach a fully developed flow regime, impose the fully developed flow through a Neumann condition, i.e. vanishing diffusive momentum flux in the streamwise direction (or, at an inflow boundary, through a Dirichlet condition, as already done here because doing otherwise saves little length of the finite element domain).
2. If a linear asymptotic analysis is available for the relaxation of the flow into the fully developed regime, use it to construct a Robin condition, or boundary condition of the third kind, for the open flow boundary. Typically this permits the finite element domain to be shortened from what is needed for comparable accuracy when a Neumann condition (or, alternatively at an inflow boundary, a Dirichlet condition) appropriate to fully developed flow is imposed.[9]
3. If no linear asymptotic analysis is available, but equations for a non-linear asymptotic regime can be set up and reduced to a one-dimensional problem, e.g. an approximate film profile equation and boundary conditions, match this problem to the main, two-dimensional problem at the open flow boundary of the latter; and then solve the two problems simultaneously, for they are necessarily coupled by continuity of mass flux, momentum flux, and stream surfaces.[19]

The matching strategy, which is the key to dividing a coating flow into different zones, is shown in Figure 9 for the upstream region where the curtain is generated. In the sheet-forming zone around the lip of the die two-dimensional analysis is needed and the velocity $\mathbf{v} = \mathbf{i}u + \mathbf{j}v$, pressure p, and free surface locations $\mathbf{x}_{FS}$ are all expanded appropriately in the finite element basis functions, as noted in Figure 9. In the curtain flow zone downstream the curtain continues to accelerate and approach purely extensional flow as it falls under gravity. For this developing flow there are asymptotic, one-dimensional, coupled, non-linear, differential equations for the curtain thickness H and midsurface inclination Θ as functions of distance s along the sheet.[27] The Galerkin/finite element method is advantageous for this equation system too, and so the two unknowns are expanded in one-dimensional, quadratic basis functions. That mass flux and total momentum flux be continuous at the matching plane implies that the inflow boundary conditions for the asymptotic equations are the outflow boundary conditions for the two-dimensional flow problem. (Comparison tests[19] show the practice of imposing the matching condition on viscous stress makes total momentum flux continuous to a closer approximation than imposing the condition on the latter.)

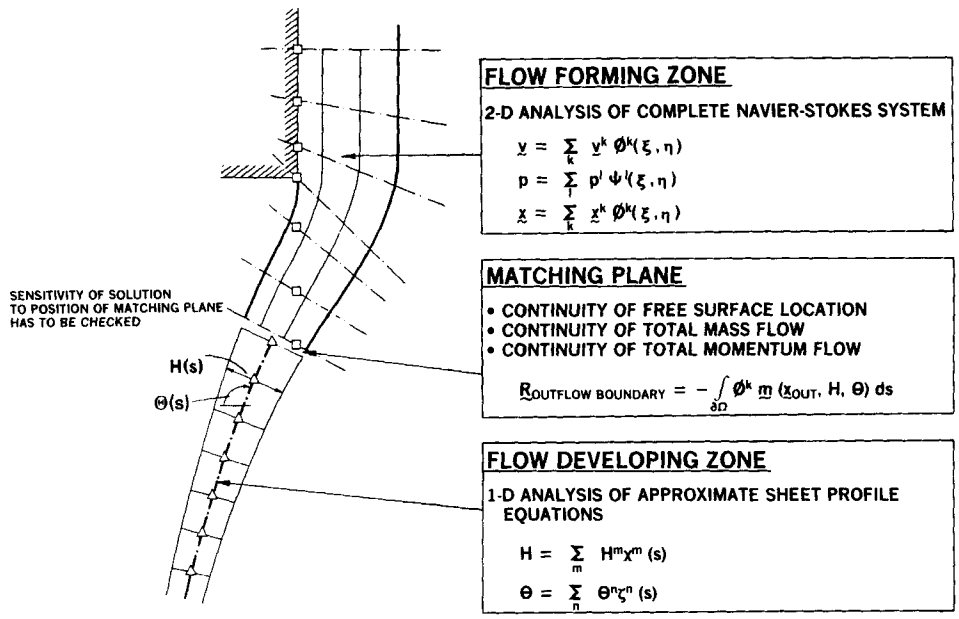

Figure 9. Matching strategy for multiple flow zones: example from curtain coating

Regardless of the way an open flow boundary is handled, the sensitivity of calculated predictions to the location of the boundary plane has to be checked and that location shifted, if necessary, until its effect is negligible. This can be handled adaptively and automatically.

The kinematic condition that no liquid crosses a free surface (or internal interface) can be regarded as an essential boundary condition. Nevertheless it is advantageous to work with weighted residuals of the kinematic conditions, namely $R_K^k \equiv \int \phi^k(\xi, \eta = \pm 1)\mathbf{n} \cdot \mathbf{v}\, ds$ where the integral extends over the free surface. Because the basis functions ϕ^k are Lagrange polynomials with the property that $\sum \phi^k = 1$, all of the equations $R_K^k = 0$ when summed yield $\int \mathbf{n} \cdot \mathbf{v}\, ds = 0$ which is plainly in accord with the requirement of global as well as element-level mass conservation. Incidentally, to evaluate the weighted residuals R_K^k, the unit normal $\mathbf{n}$ is computed only at the Gauss points of the numerical integration.

In order to prescribe the dynamic contact angle θ_D at a dynamic contact line, the vanishing of the kinematic boundary residual that is weighted by the basis function belonging to the contact line node has to be discarded and replaced by $\mathbf{n} \cdot \mathbf{n}_W = \cos \theta_D$, where $\mathbf{n}$ is the normal to the free surface and $\mathbf{n}_W$ is the normal to the substrate, both at the contact line. There is a less successful alternative that has been employed in the past. That is to use for the replacement the $\mathbf{n}$-component of the momentum residual weighted by the basis function $\phi^k(\xi, \eta)$ belonging to the same node, with $\mathbf{n}$ making exactly the angle θ_D with $\mathbf{n}_W$; the result, especially at high capillary numbers, is a distorted free surface near the contact line and a computed dynamic contact angle that differs substantially from the prescribed one.

COMPUTATION OF COEFFICIENTS OF BASIS FUNCTIONS

With the Galerkin/finite element reduction of the governing equations there are as many algebraic equations for vanishing components of $\phi^k(\xi, \eta)$-weighted momentum residuals as there are velocity component coefficients of biquadratic basis functions ϕ^k (see Figure 9).

Likewise there are as many vanishing $\psi^l(\xi, \eta)$-weighted mass residuals $R_C^l \equiv \int \psi^l \nabla \cdot \mathbf{v}\, dV$ as there are pressure coefficients of bilinear basis functions ψ^l; and as many vanishing $\phi^k(\xi, \eta = \pm 1)$ weighted kinematic residuals $R_K^k \equiv \int \phi^k(\xi, \eta \pm 1)\mathbf{n} \cdot \mathbf{v}\, ds$ as there are free surface coefficients h^k in $\mathbf{x}^k(\mathbf{h})$ (see Figure 6). The same is true of residuals and coefficients associated with the approximate sheet profile equations (see Figure 9). Thus the set of equations is complete for simultaneously calculating the velocity and pressure fields, free surface location, and profile of the asymptotically accelerating curtain.

Even at zero Reynolds number, i.e. vanishing non-linear effect of momentum convection, a free surface generally makes the equation set non-linear and so to predict a steady flow state requires an iterative computation that converges to that state. From the first finite element analysis of viscous free surface flow[28] until recently the location of a free surface has been sought by successive approximation techniques in which the location is updated on the basis of a boundary condition that is ignored during the calculation of the flow field. But it is now clear[18,29] how to employ the full Newton iteration process to solve the entire set of equations simultaneously for free surface location as well as velocity, pressure, and asymptotic profile—a grand Newton iteration that provides strikingly improved rate of convergence. This is a key to efficient prediction of coating flows.

Written in terms of a vector of finite element coefficients $\boldsymbol{\alpha}$ and a vector of weighted residuals $\mathbf{R}(\boldsymbol{\alpha})$, the Newton iteration process is of course the repeated solution of the system of linearized equations

$$\mathbf{J}[\boldsymbol{\alpha}_{n+1} - \boldsymbol{\alpha}_n] = -\mathbf{R}(\boldsymbol{\alpha}_n), \qquad \mathbf{J} \equiv \partial \mathbf{R}/\partial \boldsymbol{\alpha}$$

For the problem pictured in Figure 9 the structures of the column vector of all the residuals and of the matrix of contributions to the Jacobian matrix $\mathbf{J}$ at element level are detailed in Figure 10. The crux is the fourth column of the contribution to the Jacobian from each element, i.e. the 'element stiffness matrix'. That part of the Jacobian consists of the sensitivities of x- and y-components of weighted momentum residuals and weighted continuity and kinematic residuals to the locations of the free surface nodes in the spine parametrization. Only elements that adjoin free surfaces (or interfaces) contribute to the weighted kinematic residual. Only for elements that change shape by the isoparametric mapping as iteration proceeds are the sensitivities $\partial \mathbf{R}/\partial \mathbf{h}$ to the free boundary parameters not

RESIDUAL VECTOR	WEIGHTED RESIDUAL	WEIGHTING FUNCTION	CORRESPONDING UNKNOWN COEFFICIENTS	ELEMENT STIFFNESS MATRIX
$R_{M,x}$	x-MOMENTUM	$\phi^k(\xi,\eta)$	u^k	$\frac{\partial R_{M,x}}{\partial u}$ $\frac{\partial R_{M,x}}{\partial v}$ $\frac{\partial R_{M,x}}{\partial Q}$ $\frac{\partial R_{M,x}}{\partial h}$
$R_{M,x}$	y-MOMENTUM	$\phi^k(\xi,\eta)$	v^k	$\frac{\partial R_{M,y}}{\partial u}$ $\frac{\partial R_{M,y}}{\partial v}$ $\frac{\partial R_{M,y}}{\partial Q}$ $\frac{\partial R_{M,y}}{\partial h}$
R_C	CONTINUITY	$\psi^l(\xi,\eta)$	p^l	$\frac{\partial R_C}{\partial u}$ $\frac{\partial R_C}{\partial v}$ 0 $\frac{\partial R_C}{\partial h}$
R_K	KINEMATIC B.C.	$\phi^k(\xi, \eta = \pm 1)$	$h^k_T, h^k_B, \ldots$	$\frac{\partial R_K}{\partial u}$ $\frac{\partial R_K}{\partial v}$ 0 $\frac{\partial R_K}{\partial h}$
G	MATCHING CONDITIONS	—	H^l, Θ^l	
$R_{A,t}$	AVERAGED TANGENTIAL MOMENTUM	$x^m(s)$	H^m	$\frac{\partial R_{A,t}}{\partial H}$ $\frac{\partial R_{A,t}}{\partial Q}$
$R_{A,n}$	AVERAGED NORMAL MOMENTUM	$\zeta^n(s)$	Θ^n	$\frac{\partial R_{A,n}}{\partial H}$ $\frac{\partial R_{A,n}}{\partial Q}$

Figure 10. Overview of grand Newton iteration for evaluating coefficients of all finite element basis functions simultaneously

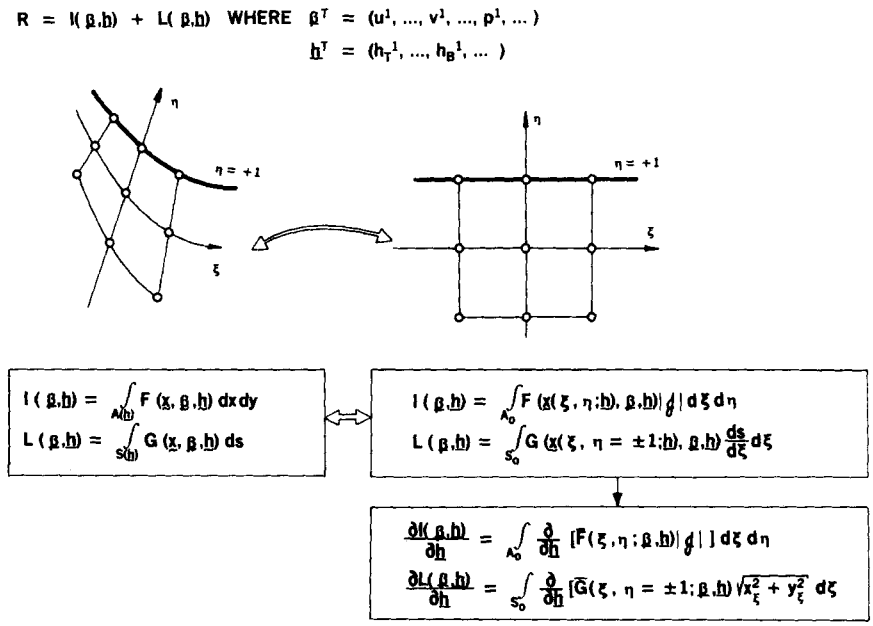

Figure 11. Evaluation of sensitivities of weighted area and line residuals to free boundary parameters

zero. (For the elements adjoining matching planes there are additional sensitivities that are not represented in Figure 10.) The key to evaluating these Jacobian entries was found by Saito.[29]

By examining the surface and line integrals (from the volume and surface integrals of the two-dimensional flow) in the weighted residuals as expressed in the (ξ, η)-computational domain, it is found that the needed derivatives can be derived in relatively straightforward fashion. Doing so requires recognizing the role of the Jacobian $\mathcal{J}(\xi, \eta)$ of the local isoparametric mapping of the standard (ξ, η)-square into the quadrilateral (x, y)-element, and of the scale factor s_ξ ($\xi, \eta = +1$ or $= 1$) of the associated mapping of an edge of the square into the free surface of an element that adjoins the free surface. The formulae for the needed derivatives are displayed in symbolic form in Figure 11 (cf. References 6, 29). $\boldsymbol{\beta}$ is the column vector of finite element coefficients of the velocity and pressure fields, i.e. the set $\{\mathbf{u}, \mathbf{v}, \mathbf{p}\}$; and $\mathbf{h}$, described above, represents the entire set of coefficients and parameters that define free boundary shapes and spine placement. In the computational domain, the basic integrals are over the fixed square A_0 or fixed line segment S_0. The Jacobian of the mapping is of course

$$\mathcal{J} \equiv \frac{\partial(x, y)}{\partial(\xi, \eta)} = \begin{vmatrix} \partial x/\partial\xi & \partial x/\partial\eta \\ \partial y/\partial\xi & \partial y/\partial\eta \end{vmatrix}$$

and the derivatives of the entries can be evaluated from

$$\frac{\partial}{\partial \mathbf{h}}\left(\frac{\partial \mathbf{x}}{\partial \xi}\right) = \sum_k \frac{\partial \mathbf{x}^k(\mathbf{h})}{\partial \mathbf{h}} \frac{\partial \phi^k}{\partial \xi}, \qquad \frac{\partial}{\partial \mathbf{h}}\left(\frac{\partial \mathbf{x}}{\partial \eta}\right) = \sum_k \frac{\partial \mathbf{x}^k(\mathbf{h})}{\partial \mathbf{h}} \frac{\partial \phi^k}{\partial \eta}$$

The derivatives $\partial \mathbf{x}^k/\partial \mathbf{h}$ in turn are found readily from $\mathbf{x}^k(\mathbf{h})$ (shown in Figure 4).

Now, in theory, Newton's method, correctly formulated and executed, approaches quadratic convergence rate as successful iteration proceeds.[30] With the complete Jacobian or global stiffness matrix $\mathbf{J}$, not only has this proved true in practice: it has proved to be an acute test of completeness and correctness of the Jacobian and so is routinely demanded of any program used to implement the coating flow theory.

Compared to successive approximation and Piccard schemes used previously, the grand Newton iteration, i.e. when free boundaries, spine placement, and even an asymptotic regime are all changing from iteration to iteration, generally converges in far fewer iterations and does so over wide parameter ranges.[25] In particular, in the capillary number range around $Ca = 1$, where many coating processes operate, successive approximations to free surface shape, whether based on iterating on the kinematic condition[28,15] or the normal stress boundary condition,[2,15] converge slowly and sometimes succeed only with the aid of artful 'underrelaxation'.

The Jacobian of a converged solution returns added benefits. It is valuable for (i) estimating the new solution $\boldsymbol{\alpha}_0(\boldsymbol{\Pi}^N)$ to start iteration when the parameter set is changed from $\boldsymbol{\Pi}^{N-1}$ or $\boldsymbol{\Pi}^N$, i.e. for first-order continuation; (ii) assessing the sensitivity of the flow state, i.e. a converged solution, to parameters; and (iii) analysing the stability of the flow state to small disturbances.[31]

Another key to prediction of a coating flow is finding a start-up approximation $\boldsymbol{\alpha}_0(\boldsymbol{\Pi}^1)$—the very first approximation when a program for a particular type of flow is ready and a likely parameter set $\boldsymbol{\Pi}^1$ has been chosen—that falls within the domain of practicable convergence rate (perhaps with the aid of 'underrelaxation' or 'overrelaxation' of Newton iteration). Because of their free surfaces, coating flows rarely have limiting cases that are linear or otherwise amenable to traditional analysis. Experience has now taught that experimental evidence; rough-and-ready physical models; and, sometimes, investing in solving some non-linear asymptotic approximation, can all be valuable in placing spines appropriately and beginning the search for a successful first approximation.

The grand Newton iteration process together with start-up and continuation procedures is diagrammed in Figure 12; further details are recorded elsewhere.[6] When a solution is sought at a new value of a parameter the simplest option is zeroth-order continuation, which means restricting the parameter change so that the solution of the last case lies well enough in the convergence domain of the new case that only a few iterations are required to achieve the degree of convergence desired.

Larger parameter changes may be possible with first-order continuation, which amounts to projection along the parametric gradient of the solution, as in Euler's method of time-integration. First-order continuation takes advantage of the information in the Jacobian matrix of the last case. All that is required is the relatively easy solution of a subsidiary problem for the continuation vector $\mathbf{d}_m$ (as indicated in Figure 12), which is then available for initializing the next case.

It has usually proved efficient to control parameter changes after start-up so that the Newton process converges (largest change less than 10^{-4} in any of the entries in $\boldsymbol{\alpha}$, all of which are of order unity excepting pressure in some cases), and does so in three to five iterations—never more than seven even in start-up, once a successful start-up approximation is found.

What follow are illustrative predictions of curtain coating flow and flow between rotating cylinders which were computed by the theory. At each iteration the linear system in Newton's method was solved by Hood's[32,33] frontal routine with minor modifications. The number of elements ranged from 30 to 100; the number of unknowns from about 400 to

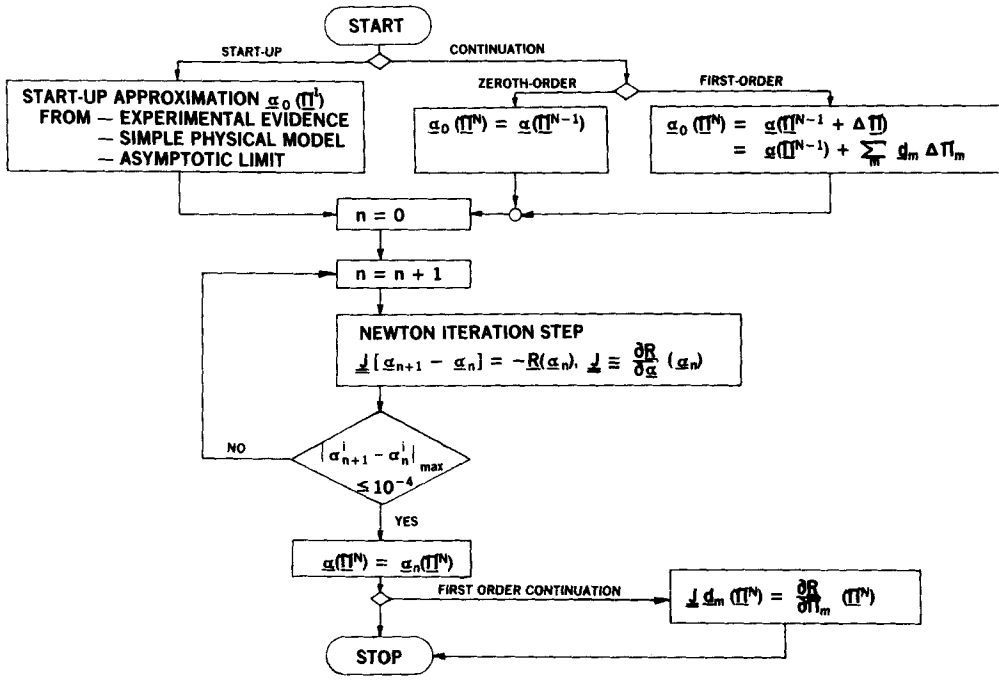

Figure 12. Summary of start-up, iteration, and continuation procedures

nearly 1500. Around 70 K octal words of core memory were used. The amount of out-of-core memory needed for the frontal routine, which was originally designed for disc memory, was up to 200 K octal words; the amount depends strongly on the front width, which is sensitive to the shape of the computational domain. Some of the predictions, mainly with the smaller numbers of unknowns, were made with a CDC Cyber 74 computer and the FTN compiler. Depending on the number of unknowns and the front width, individual iteration steps took from 5 to 12 seconds of central processor time. With the larger numbers of unknowns the calculations were made with a CRAY-1A supercomputer and took from 0·5 to 1 second per iteration.

THEORETICAL PREDICTIONS OF SAMPLE FLOWS

Calculated flows in the sheet-forming and curtain flow zones of a curtain coater[19] are shown in Figure 13. At relatively high Reynolds numbers (flow rates) the trajectory is ballistic, i.e. it resembles the path of an unimpeded body. As flow rate is diminished the trajectory reverts to antiballistic and passes through a maximum deflection. At still lower flow rates, viscous effects shorten the forming zone and the liquid curtain falls almost vertically beyond a short distance below the lip of the die. A complete finite element analysis of the flow, including configurations in which the underside of the lip is wet by the liquid, settles the causes of the curious set of phenomena known as the teapot effect.[17]

That the predictions are not sensitive to further refinement of the tessellation has been tested, but the critical test of the theory is comparison with experiment. In Figure 14 precise measurements of the outer free surface profile are compared with the predictions from Figure 13. The agreement is excellent, except at intermediate Reynolds numbers of 5 and 7,

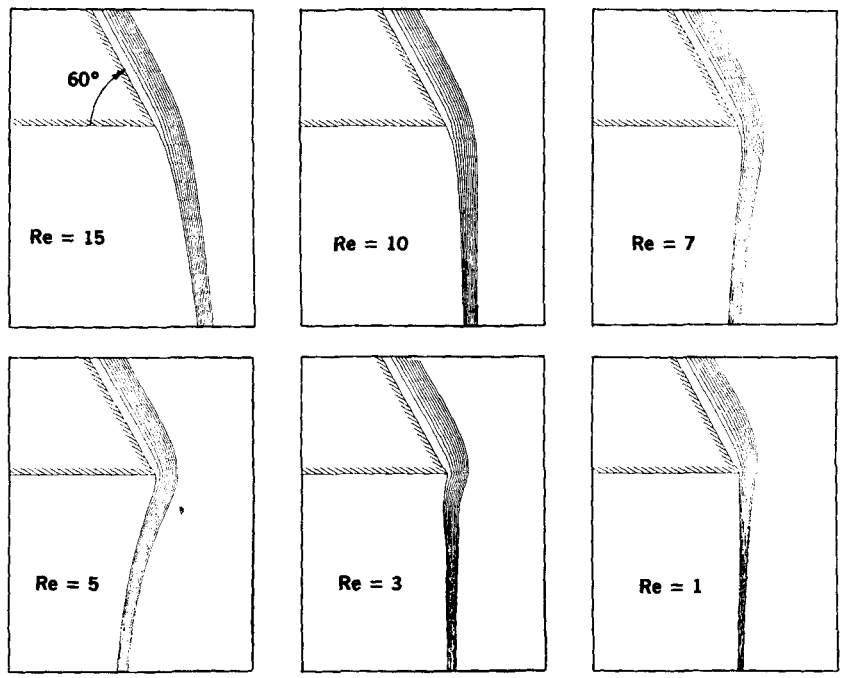

Figure 13. Deflection of liquid film falling over lip of inclined slide—'Teapot effect'. $Re \equiv \rho q/\mu$, where q is flow rate per unit width; $N_\sigma \equiv \sigma(4\mu^4 g/\rho)^{-1/3} = 1{\cdot}15$

where the deflection is greatest and the prediction most sensitive to errors in measurement of flow rate and liquid properties, as well as to slight wetting back along the underside of the lip.

Flow in the coated-film forming zone, or impinging zone, largely determines the parameter range of operability of curtain coating. Figure 15 displays a sequence of predictions at high enough capillary number, or low enough surface tension, that the apparent dynamic contact angle is determined solely by hydrodynamic forces and becomes a dependent variable.[34] As the ratio of substrate speed U to impingement speed V rises, the dynamic contact line shifts downstream and the apparent dynamic contact angle, measured through the liquid, approaches 180°. It is commonly hypothesized that 180° is the upper limit for coating without visible air entrainment.[35,36]

Consequently the predicted lines of constant apparent dynamic contact angle θ_D in the plane of Reynolds number Re and speed ratio U/V are of particular interest. Such lines are plotted in Figure 16. The points shown are conditions at which patents claim that curtain coaters have operated successfully.[34] Thus the high capillary number theory, even though it omits the effect of surface tension, appears to account well for the essential aspects of dynamic wetting at high coating speeds. Detailed understanding and accurate prediction of the air entrainment limit require more refined analysis, which is under way.

The last predictions are of flows between counter-rotating and co-rotating cylinders, such as occur in forward and reverse roll coating (see Figure 1). The simplest case is film splitting between rolls turning at equal speeds but in opposite directions. Figure 17 shows the right half of the film-splitting zone computed by Coyle.[3] Prominent is the slowly recirculating eddy, which shrinks and eventually disappears as capillary number rises, i.e. as the relative

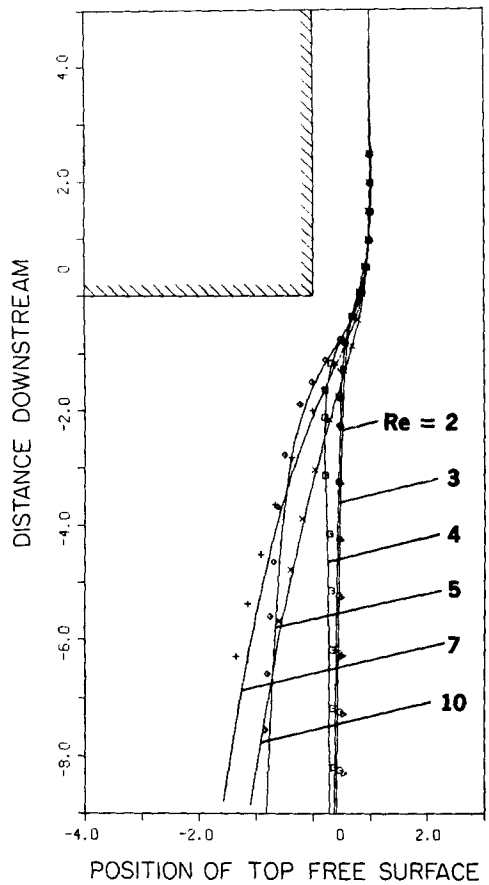

Figure 14. Predicted outer free surface profile of deflected curtain (Figure 13) compared with measured points

importance of surface tension falls. Almost all analyses of roll-coating flows have been by the so-called lubrication approximation, which did not and cannot account for the recirculating eddies. Such eddies have been detected and photographed in the laboratory, and they can have severe consequences in practical situations.

How changing the speed ratio of the rolls alters the film-splitting flow is indicated by Coyle's computations plotted in Figure 18.[3] More liquid leaves the gap on the faster-turning roll and the eddy pattern distorts. At a speed ratio of 2·5 one eddy is gone and the other is much weakened.

The flows in Figures 17 and 18 can occur on the downstream side of the nip between 'forward-turning' rolls. Examples of flow fields on the upstream side of the nip, the so-called 'back bead', are displayed in Figure 19.[37] In the diagram above, the upper roll is stationary so that the contact line on it is static. The main liquid stream follows closely the moving roll but drives a prominent eddy. In the diagram below, both rolls are turning at the same speed and the liquid comes in contact with the upper roll at a dynamic contact line. The eddy structure is greatly altered and there is a remarkable S-bend in the streamlines of arriving liquid that wends its way to the neighbourhood of the upper roll surface. The rest of the incoming film follows the surface of the lower roll. But in the flow field are two contra-rotating eddies, which here as in other two-dimensional flows represent trapped material.

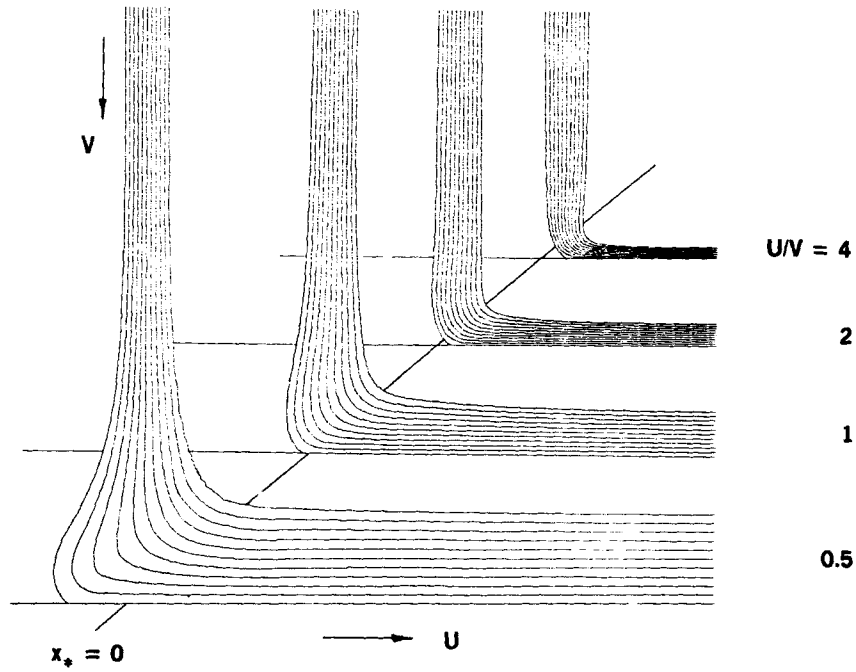

Figure 15. Streamlines in impinging zone of curtain coating, with increasing ratio of substrate speed U to impinging velocity V. $Re \equiv \rho q/\mu = 2{\cdot}5$, where q is flow rate per unit width, $Ca \equiv \mu U/\sigma \to \infty$

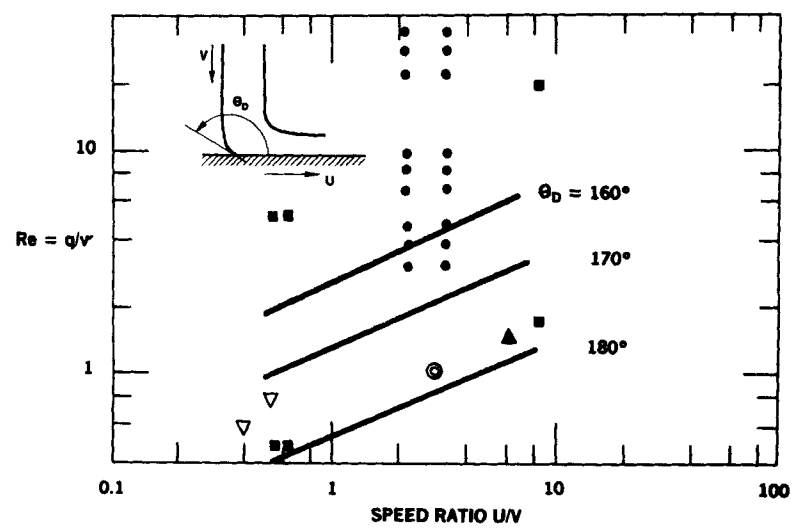

Figure 16. Impinging zone of curtain coating: lines of constant apparent dynamic contact angle and points of successful curtain coating according to patents. $Ca \equiv \mu U/\sigma \to \infty$

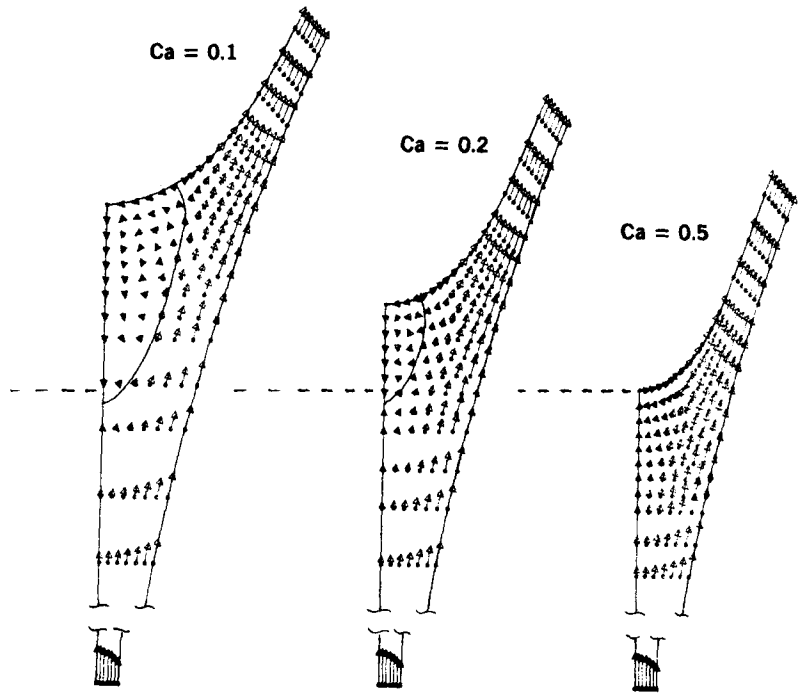

Figure 17. Symmetrical film splitting between counter-rotating rolls: right half of flow field. $Re = 0$; $D/h_0 = 100$, where D is roll diameter and h_0 is the minimum distance between their surfaces

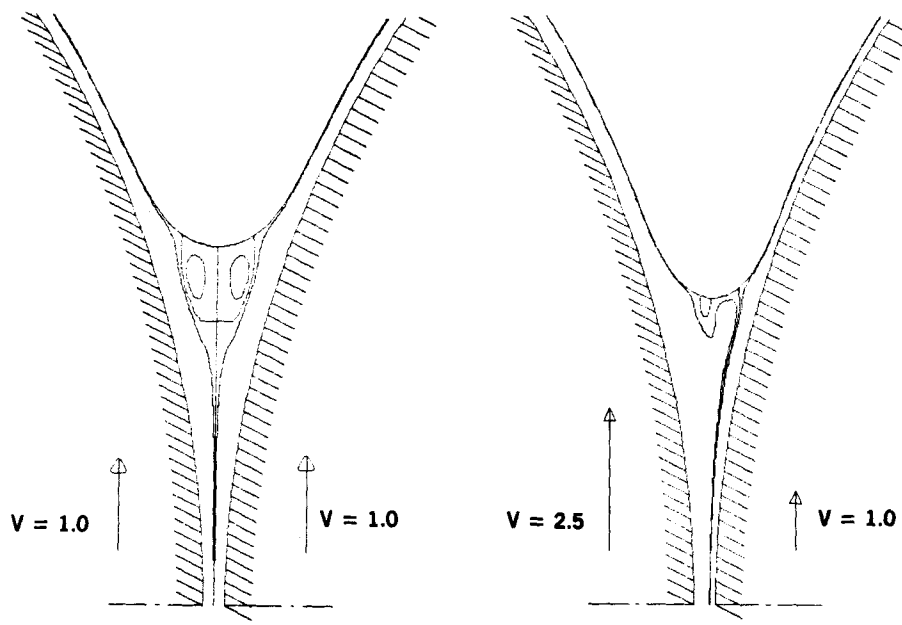

Figure 18. Streamlines in symmetrical and asymmetrical film splitting between rolls. $Ca = 0{\cdot}1$; $Re = 0$; $D/h_0 = 100$

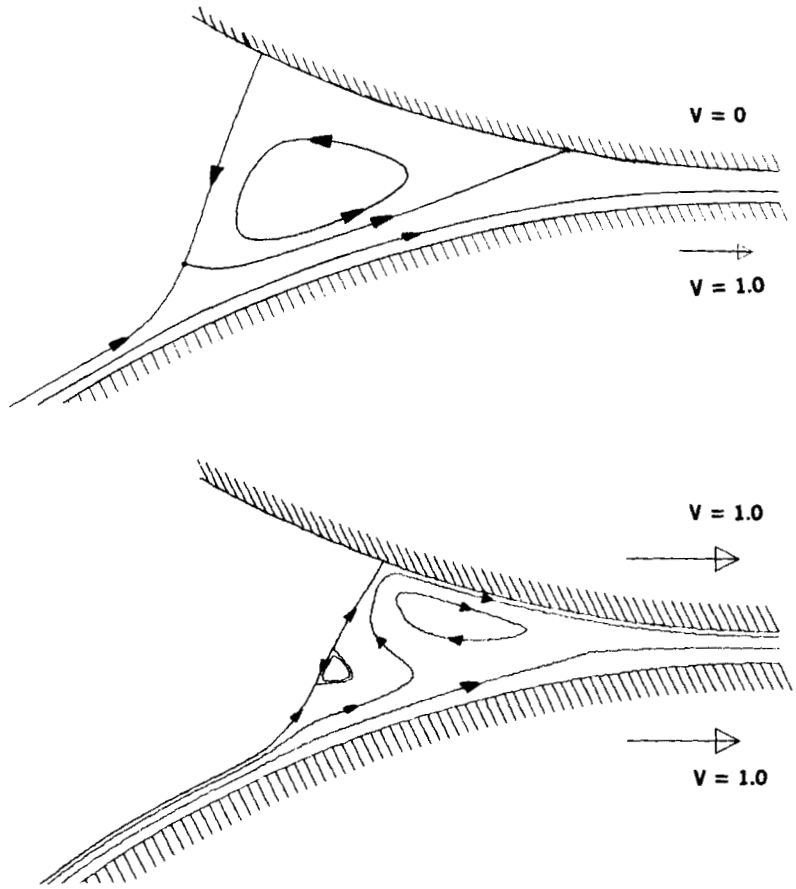

Figure 19. Streamlines in back bead or rolling bank of forward roll coater. $Ca = 0{\cdot}11$; $Re = 0$; $D/h_0 = 100$

These several cases of flow between rolls were actually steps along a path that continued to the goal of theory of reverse roll coating,[4] an example of which is shown in Figure 20. Liquid arrives from the right on the lower roll. The portion of the incoming flow near the roll surface passes directly through the nip and departs as the film at lower left. Liquid a little higher up in the incoming flow also passes through the nip but goes to wet the dry upper roll surface (or surface of a flexible substrate carried by the roll) at the dynamic wetting line; then it is carried back through the nip and exits deep in the film leaving at the upper right. Liquid at the top of the incoming flow never reaches the nip, but skirts a large eddy and resurfaces at the top of the film leaving at upper right. Besides the large, recirculating eddy on the right, which has been seen, there is a small, unexpected one on the left side of the nip.

What is most intriguing about the flow field shown in Figure 20 is the rapidly varying sequence of deformations and deformation rates a parcel of liquid experiences as it passes through the various flow zones.[4] The numbers tabulated are shear rates and extension rates in the Newtonian flow of a liquid parcel that passes through the nip close to the surface of the lower roll. The experience of a parcel that passes close to the dynamic wetting line can be far more severe and is sensitive to the local slip regime. In high-speed coating passage times through the nip can be much less than 0·1 s. These calculations bring out the intensity,

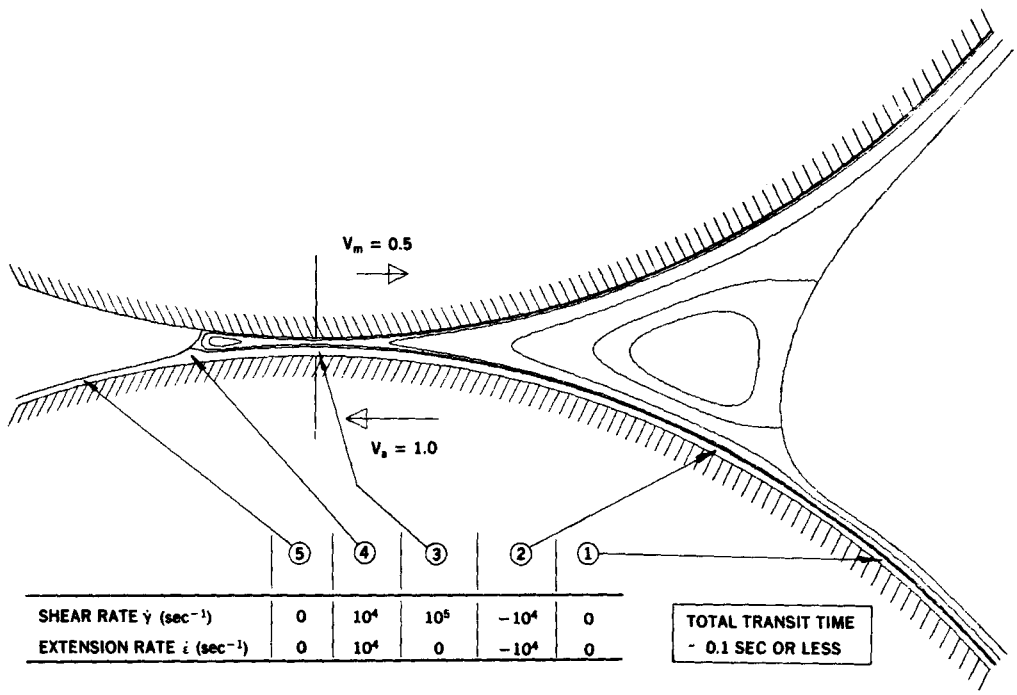

Figure 20. Streamlines and deformation rates of various flow regions in reverse roll coating. $Ca = 0{\cdot}1$; $Re = 0$; $V_m/V_a = 0{\cdot}5$; $D/h_0 = 100$, where D is roll diameter and h_0 is the minimum distance between rolls

transience, and complexity of liquid deformation that is typical not only of flows between rolls, but also of the forming zones of most other coating flows (compare Figure 1).

One question the theoretical predictions immediately raise is whether liquids that respond as Newtonian in conventional rheological testing always behave as Newtonian in the forming zones of coating flows.

CONCLUSION

These sample results illustrate the power and effectiveness of the coating flow theory based on finite element and asymptotic analysis. Recent advances make the finite element treatment of viscous free surface flows more efficient and more generally applicable: spine parametrization of free boundaries; systematic isoparametric mapping; adherence to mass flux and total momentum flux formulations, especially in dealing with free boundaries and open flow boundaries; systematic use of surface and volume divergence theorems in order to impose free surface boundary conditions in their natural form; size reduction of computational domain by means of boundary conditions derived from asymptotic analysis or by matching to one-dimensional finite element solutions of asymptotic equations; full Newton iteration of the entire set of algebraic equations; and parameter continuation methods to trace out trees of solutions of the usually highly non-linear equation sets of the discretized, free boundary flow problems.

The theory yields detailed predictions of free surface and interface shapes, velocity fields and associated strain-rate and vorticity fields—thereby revealing unwanted eddies and slow

flow regions, for example—as well as pressure and viscous stress fields. The predictions can be used for rheological purposes. They can be used to investigate effects of changing the design of the coating die, its relationship to the substrate, and other operating variables. They can be used to reveal the physical mechanisms of practically important aspects of coating processes, such as bounds on operability. These predictive capabilities are all the more important because the small scale and complexity of most coating flows makes flow visualization difficult, important local details experimentally inaccessible, and accurate measurement formidable—especially measurement of dynamical quantities.

Further developments are in the offing, some of them already far along in the research programme at the University of Minnesota, some of them being pursued by several research groups around the world. The theory will be made even more flexible and also more accessible to non-specialist users by schemes of automatic, adaptive spine placement, domain tessellation, and tessellation refinement in regions of steepest gradients in the flow field.[38] Advancing understanding of the physics of wetting and of contact lines will be incorporated into the theory.[11,12] Once a steady, two-dimensional flow state is predicted, extremely important issues are its response to small disturbances and its uniqueness, issues that call for analysis of stability and bifurcation.[39,40] Unsteady flow states of start-ups and upsets (such as those caused by substrate splices passing by) require analysis of unsteady coating flows.[22,41] Successful coating flows are two-dimensional except near the edges of the flows: various of the edge effects are practically important and deserve three-dimensional analysis. Many coating processes deposit non-Newtonian liquids, and although shear-thinning is easily handled by the current theory,[3,4,19] incorporating visco-elastic phenomena remains a challenge.[42] Many liquids being coated contain surface-active agents and volatile constituents,[43] the effects of which require incorporating mass transfer, heat transfer, and surface-tension-gradient effects into what is basically a fluid mechanical theory.

ACKNOWLEDGEMENT

Financial support was provided by the U.S. National Science Foundation, the University of Minnesota Computer Center, and grants-in-aid from the Eastman Kodak Company and 3M Company. D. J. Coyle contributed valuable discussions as well as predictions of roll coating flows.

REFERENCES

1. K. J. Ruschak and L. E. Scriven, 'Rimming flow of liquid in a rotating horizontal cylinder', *J. Fluid Mech.*, **76,** 113 (1976).
2. F. M. Orr and L. E. Scriven, 'Rimming flow: numerical simulation of steady viscous free-surface flow with surface tension'. *J. Fluid Mech.*, **84,** 145 (1978).
3. D. J. Coyle, C. W. Macosko and L. E. Scriven, 'Computer simulation of nip flow in roll coating', in T. Provder (ed.) *Computer Applications in Applied Polymer Science*, ACS Symposium Series 197, American Chemical Society, Washington, 1982.
4. D. J. Coyle, C. W. Macosko and L. E. Scriven, 'Finite element analysis of reverse roll coating', *Paper 101h, AIChE Ann. Mtg.*, Los Angeles, 14–18 November 1982.
5. S. F. Kistler and L. E. Scriven, 'Coating flow theory by finite element and asymptotic analysis of the Navier–Stokes system', in T. Kawai (ed.) *Finite Element Flow Analysis; Proc. Fourth Int. Symp. on Finite Element Methods in Flow Problems*, University of Tokyo Press, 1982.
6. S. F. Kistler and L. E. Scriven, 'Coating flow computations', in J. R. A. Pearson and S. M. Richardson (eds) *Computational Analysis of Polymer Processing*, Applied Science Publishers, London, 1983.
7. S. F. Kistler and L. E. Scriven, 'Finite element analysis of formation of film flowing down an inclined plane', to be submitted (1983).
8. B. G. Higgins, 'Downstream development of two-dimensional viscocapillary film flow', *I & EC Fundam.*, **21,** 168 (1982).

9. N. E. Bixler and L. E. Scriven, 'Robin conditions for open flow boundaries', to be submitted (1984).
10. L. E. Scriven, 'How does air entrain at wetting lines?', *Chem. Eng. Comm.*, submitted (1983).
11. G. F. Teletzke, H. T. Davis and L. E. Scriven, 'Wetting hydrodynamics', *J. Fluid Mech.*, in review (1983).
12. K. Miyamoto and L. E. Scriven, 'Breakdown of air film entrained by liquid coated on web', *Paper 101g, AIChE Ann. Mtg.*, Los Angeles, 14–18 November 1982 (to be submitted to *AIChE Journal*).
13. C. Huh and L. E. Scriven, 'Hydrodynamic model of steady movement of a solid/liquid/fluid contact line', *J. Coll. Interf. Sci.*, **35,** 85 (1971).
14. C. Huh and S. G. Mason, 'The steady movement of a liquid meniscus in a capillary tube', *J. Fluid Mech.*, **81,** 401 (1977).
15. W. J. Silliman and L. E. Scriven, 'Separating flow near a static contact line: slip at a wall and shape of a free surface', *J. Comp. Phys.*, **34,** 287 (1980).
16. D. H. Michael, 'The separation of a viscous liquid at a straight edge', *Mathematika*, **5,** 82 (1958).
17. S. F. Kistler and L. E. Scriven, 'The teapot effect: Finite element analysis and experimental study of the deflection, wetting and hysteresis phenomena in two dimensions', to be submitted (1983).
18. K. J. Ruschak, 'A method for incorporating free boundaries with surface tension in finite element fluid-flow simulators', *Int. J. Num. Meth. Eng.* **15,** 639–648 (1980).
19. S. F. Kistler, 'The fluid mechanics of curtain coating and related viscous free surface flows with contact lines', *Ph.D. Thesis*, University of Minnesota, 1983.
20. P. S. Huyakorn, C. Taylor, R. L. Lee and P. M. Gresho, 'A comparison of various mixed interpolation finite elements in the velocity-pressure formulation of the Navier–Stokes equations', *Comp. and Fluids*, **6,** 25 (1978).
21. R. L. Sani, P. M. Gresho, R. L. Lee and D. F. Griffiths, 'The cause and cure (?) of the spurious pressures generated by certain FEM solutions of the incompressible Navier–Stokes equations', part I., *Int. J. Num. Meth. Fluids*, **1**, 17–43 (1981); part 2, **1**, 171–204 (1981).
22. H. S. Khesghi and L. E. Scriven, 'Penalty-finite element analysis of time-dependent two-dimensional free surface film flow', in T. Kawai (ed.) *Finite Element Flow Analysis; Proc. Fourth Int. Symp. on Finite Element Methods in Flow Problems*, University of Tokyo Press, 1982.
23. G. Strang and G. J. Fix, *An Analysis of the Finite Element Method*, Prentice-Hall, Englewood Cliffs, 1973.
24. O. C. Zienkiewicz, *The Finite Element Method*, McGraw-Hill, London, 1977.
25. H. Saito and L. E. Scriven, 'Study of coating flow by the finite element method', *J. Comp. Phys.*, **42,** 53 (1981).
26. M. S. Engelman, R. L. Sani and P. M. Gresho, 'The implementation of normal and/or tangential boundary conditions in finite element codes for incompressible fluid flow', *Int. J. Num. Meth. Fluids*, **2,** 225–238 (1982).
27. S. F. Kistler and L. E. Scriven, 'First order approximation of flow in viscous liquid sheets', to be submitted (1983).
28. R. E. Nickell, R. I. Tanner and B. Caswell, 'Solution of viscous incompressible jet and free surface flows using finite element methods', *J. Fluid Mech.* **65,** 189 (1974).
29. H. Saito and L. E. Scriven, 'Newton method for finite element analysis of viscous free surface flow', *Int. J. Num. Meth. Fluids*, to be submitted (1983).
30. E. Isaacson and H. B. Keller, *Analysis of Numerical Methods*, Wiley, New York, 1966.
31. R. A. Brown, L. E. Scriven and W. J. Silliman, 'Computer-aided analysis of nonlinear problems in transport phenomena', in P. J. Holmes (ed.), *New Approaches to Nonlinear Problems in Dynamics*, SIAM, Philadelphia, 1980, p. 298.
32. P. Hood, 'Frontal solution program for unsymmetric matrices', *Int. J. Num. Meth. Eng.*, **10**, 379–399 (1976).
33. P. Hood, 'Note on frontal solution program for unsymmetric matrices', *Int. J. Num. Meth. Eng.* **11,** 1055 (1977).
34. S. F. Kistler and L. E. Scriven, 'Finite element analysis of dynamic wetting for curtain coating at high capillary numbers', *Paper 45d, AIChE Nat'l. Mtg.*, Orlando, 28 February–3 March 1982.
35. E. B. Gutoff and C. E. Kendrick, 'Dynamic contact angles', *AIChE Journal*, **28,** 459 (1982).
36. T. D. Blake and K. J. Ruschak, 'A maximum speed of wetting', *Nature*, **282,** 489 (1979).
37. D. J. Coyle, 'The fluid dynamics of roll-coating—steady flows, stability and rheology', *Ph.D. Thesis*, University of Minnesota (1984).
38. R. E. Benner and L. E. Scriven, 'Adaptive subdomaining for solution of one-dimensional problems by the finite element method', *SIAM 30th Anniversary Meeting*, Stanford, 19–23 July 1982.
39. K. J. Ruschak, 'Linear stability analysis for free boundary flows by the finite element method', *Preprint 47f, AIChE Nat'l. Mtg.*, Orlando, 28 February–3 March 1982.
40. N. E. Bixler and L. E. Scriven, 'Stability of slot and knife coating by finite element analysis', *Paper 47e AIChE Nat'l. Mtg.*, Orlando, 28 Febraury–3 March 1982.
41. H. S. Kheshgi and L. E. Scriven, 'Penalty finite element analysis of unsteady disturbed film flow on an inclined plate', *Paper 21d, AIChE Ann. Mtg.*, Los Angeles, 14–18 November 1982.
42. A. C. Papanastasiou, C. W. Macosko and L. E. Scriven, 'An integral constitutive equation for mixed flows. Viscoelastic characterization', *J. Rheology*, **27,** 387–410 (1983).
43. G. S. Sterzi, 'Surfactant effect in film flow', *M.S. Thesis*, University of Minnesota (1982).